Identifying parameters of a discrete numerical model of soil from a geotechnical field test

Ali Abdallah, Rodaina Aboul Hosn, Bilal Al Tfaily, Luc Sibille

Identifying parameters of a discrete numerical model of soil from a geotechnical field test

Ali Abdallah[a,b,*], Rodaina Aboul Hosn[b], Bilal Al Tfaily[c], Luc Sibille[c]

[a] *Université de Lyon, Ecole centrale de Lyon, LTDS, UMR CNRS 5513, 36 avenue Guy deCollongue, 69134 Ecully, France.*
[b] *Université Paris-Est, Institut de Recherche en Constructibilité, ESTP, 28 avenue du Président Wilson, 94234 Cachan, France.*
[c] *Univ. Grenoble Alpes, CNRS, Grenoble INP, 3SR, F-38000 Grenoble, France.*

Abstract

A discrete numerical model of a pressuremeter test was developed in this paper. The model is constituted of spherical particles with a contact law involving an inter-particle rolling resistance in addition to the classical Coulomb friction model. The model is calibrated from a pressuremeter test performed in the Hostun sand. An adaptive size of discretization of the soil domain is considered to limit the computational cost. Different parameter sets are defined to identify the initial density of the numerical granular assembly. Then, each parameter set leads to a different calibration of the mechanical parameters of the model in order to reproduce the pressuremeter test results. Simulations show that experimental data from a pressuremeter test alone are not enough to fully calibrate the discrete model. Other laboratory test results need to be considered in the calibration methodology. Eventually, the prediction capability of the model is assessed by comparing the simulated constitutive responses to those measured experimentally on different triaxial loading paths.

Keywords:
Discrete element method, Pressuremeter test, Boundary value problem, Granular material

1. Introduction

Since the introduction of the Discrete Element Method (DEM) by Cundall and Strack (1979) to model the behavior of granular materials, this method has been widely applied in geomechanics. Numerical experiments have been done in order to study the constitutive behavior of geomaterials at a representative elementary volume (REV) scale (e.g. Bardet 1994; Ciantia et al. 2016) as well as the underlying mechanism at the grain scale (for instance Iwashita and Oda 2000; Rajaï et al. 1996). DEM models have also proven to be able to predict not only qualitatively but also quantitatively the behavior of soils even once subjected to complex loading paths (Sibille et al., 2019). Eventually, geotechnical engineering problems are addressed with a discrete approach which is rather efficient when large deformations are expected or failure and post failure responses are investigated (Li et al., 2019; Villard et al., 2016). When

*Corresponding author
Email address: ali.abdallah@ec-lyon.fr (Ali Abdallah)

it comes to the calibration of a DEM model, this usually requires a characterization of the soil mechanical properties through laboratory experiments such as triaxial or direct shear tests. However, such experiments are not necessarily representative of the properties of the in-situ soil. Most often, in an engineering context, mechanical properties of soils are deduced from field tests such as the static penetrometer or the pressuremeter tests. It is therefore important to propose a methodology for calibrating DEM models based on field tests.

Identifying model parameters directly from field tests has been already investigated in the context of continuum modeling with elasto-plastic constitutive relations (Boubanga, 1990; Bahar, 1992; Zentar et al., 2001). One of the conclusion from these studies is that the set of model parameters to simulate the field test results is not unique as found by Fahey and Carter (1993), and a choice should be made among the different parameter sets able to reproduce the field test data. For an elastic-perfectly plastic model involving eight mechanical parameters, Biarez et al. (1998) suggested to use information from laboratory tests, like the triaxial test, in addition to pressuremeter data in order to be able to fully calibrate the model.

Concerning the DEM approach, numerical models of field tests as cone penetration tests and pressuremeter tests have already been developed (Butlanska et al., 2014; Huang and Ma, 1994; Hosseini-Sadrabadi et al., 2019; Geng, 2010). However, the parameters of such numerical models are usually calibrated from laboratory test results and the field test model is used as a tool to investigate and characterize the soil response to these field tests. Identification of discrete model parameters from field tests has been poorly investigated and there is still no clear methodology to achieve the parameter identification by this way. Therefore, the main objective of this paper is to study the relevance of defining a calibration methodology of a DEM model from field tests. The pressuremeter test is chosen for this study because it provides a wider range of information about the mechanical soil characteristics than a cone penetration test. The pressure-volume curve resulting from the pressuremeter test provides information about the stress-strain relationship before the soil failure and at the failure state, whereas cone resistance in conventional penetration state informs on the soil shear strength (failure) only.

This paper is organized as follows : Section 2 presents the reference pressuremeter test and the used soil. Then, in Section 3, the discrete element model, and in particular the inter-granular contact laws, are defined. Preparation of the granular assembly as well as the DEM model of the pressuremeter test (boundary conditions and probe inflation) are also discussed in this section. Thereafter, in Section 4, an investigation of the effects of the model parameters is done through a parametric study. In particular, the study focuses mainly on the influence of the initial porosity and the plastic parameters (contact friction angle φ_c and rolling friction coefficient, η_r), while the elastic parameters are presumed as they have a minor impact on the results. Subsequently, in Section 5, the criteria for choosing the initial porosity and the definition of the calibrating methodology are provided. The result obtained from the calibration of the model parameters is eventually displayed. Section 6 is devoted to the definition of the triaxial loading paths considered for the validation of the model. Prediction capability of the model, based on the suggested calibration, is assessed by comparing the simulated constitutive responses to the responses measured experimentally on these loading paths. Finally, main findings and conclusions are discussed in Section 7.

2. Reference pressuremeter test and soil

The reference pressuremeter test considered in this study is from a series of tests performed by Mokrani (1991) in Hostun sand RF within a calibration chamber under controlled conditions. The calibration chamber is 120 cm in diameter and 150 cm high and configured to apply oedometric boundary conditions (the vertical stress is imposed via an inflatable diaphragm at the top of the chamber while the vertical circular wall is fixed). The pressuremeter is constituted of a mono-cell probe with a diameter of 55 mm placed at the centre of the calibration chamber. The inflatable length of the probe is 160 mm. Soil sample is prepared by dry pluviation of the sand and the probe is buried during the sand deposition. Consequently, a direct contact between the membrane of the probe and the sand is established. After applying the specified axial stress on the soil deposit, the probe's membrane expands by fluid injection at a flow rate of 10 cm^3/min, which corresponds to a volume variation speed of 2.6 $\%/min$. The expansion stops when the probe's volume has doubled. A detailed description of the test procedure can be found in Mokrani (1991).

Hostun sand RF is composed of sub-angular to angular particles with a nearly uniform grain size distribution (Figure 1). The median grain size is $D_{50} = 0.35\ mm$ and the coefficient of uniformity is $C_U = 1.8$. The maximum and minimum void ratios are respectively $e_{max} = 0.961$ and $e_{min} = 0.624$ (Flavigny et al., 1990). The grain size distribution of Hostun sand is presented in Figure 1.

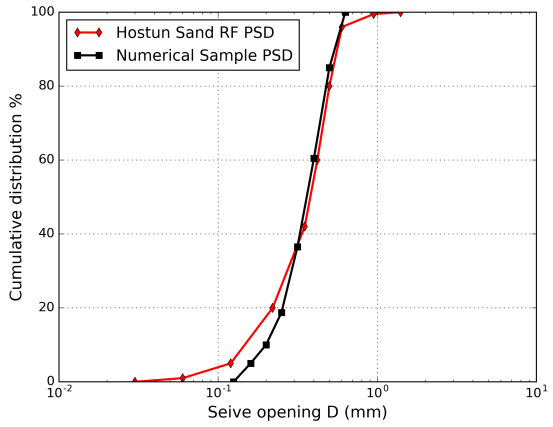

Figure 1: Particle size distribution of the Hostun sand RF used for the pressuremeter test in the calibration chamber. For comparison, the particle size distribution used for the discrete model of the pressuremeter test is also displayed

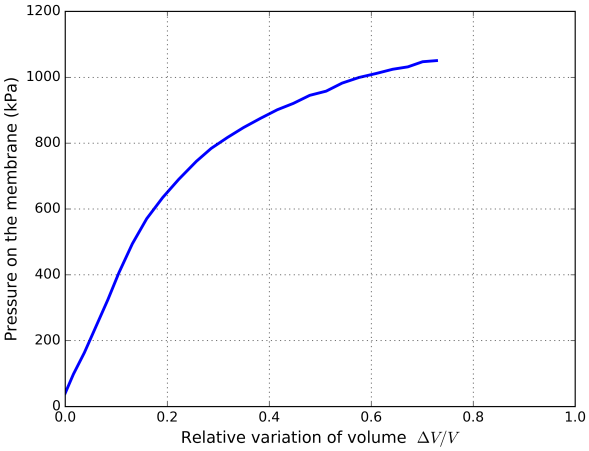

Figure 2: Pressuremeter curve of the experimental test n°11

In this study, a dense sand sample with a relative density $D_r = 83\%$ under a vertical stress equal to $\sigma_V = 100$ kPa (test n°11 from the series of Mokrani (1991)) is chosen to calibrate the discrete model. The pressure-volume curve obtained during the expansion of the probe is shown in Figure 2. In this figure, the pressure represents the pressure applied by the membrane of the probe on the soil and the volume is the volume of fluid injected in the probe (i.e.

the volume growth of the probe with respect to its initial volume). The absence of the re-establishing phase in the pressuremeter curve, representing the initial expansion of the probe until its full contact with the boundaries of the borehole when the test is performed *in situ*, is due to the direct contact between the probe and the soil thanks to the sand deposition around the probe.

3. Discrete numerical model

3.1. Inter-particle contact law

The soil is represented by an assembly of spherical particles. The interaction contact law includes Coulomb friction (Figure 3) characterized by three parameters: the normal stiffness, k_n; the tangential stiffness, k_t; and the contact friction angle, φ_c. When two spheres are in contact, normal contact force, $\vec{F}_n$, and tangential contact force, $\vec{F}_t$, to the contact plane, are calculated such that:

$$\vec{F}_n = k_n \delta_n \vec{n} \tag{1}$$

$$\Delta\vec{F}_t = -k_t \, \Delta\vec{u}_t \qquad with \qquad \| \vec{F}_t \| \leq \| \vec{F}_n \| \tan\varphi_c \tag{2}$$

where $\vec{n}$ is the normal unit vector to the plane of contact. Contact detection depends on the overlap, δ_n, between two particles. So when there is no overlap, the contact is lost. The normal contact force is directly proportional to the overlap, δ_n, through the normal stiffness, k_n. $\vec{F}_t$ is computed in an incremental form because of the non-linearity introduced by the Coulomb friction. In the elastic regime, it is directly proportional to the relative tangential displacement, $\Delta\vec{u}_t$, at contact point through the tangential stiffness, k_t.

Rolling resistance is introduced in addition to Coulomb friction in order to limit the excessive rolling of the oversimplified spherical particles and to reflect the soil grain's angularity. Representation of real grain shape, with for instance polyhedral particles, requires an important additional computational cost. Spherical particles with rolling resistance constitutes an alternative solution to describe correctly the plastic macroscopic behaviour of soils as shown in Sibille et al. (2019) while keeping a reasonable computational cost. Rolling resistance at contact is defined by the rolling stiffness, k_r, and the rolling friction coefficient, η_r, as represented in Figure 3B. The rolling moment $\vec{M}_r$ to limit the relative rolling rotation of particles at contact, $\vec{\theta}_r$, is then determined as follows:

$$\Delta\vec{M}_r = -k_r \Delta\vec{\theta}_r \qquad with \qquad \| \vec{M}_r \| \leq \| \vec{F}_n \| \, \eta_r \min(R_1, R_2) \tag{3}$$

where R_1 and R_2 are the radii of the two particles involved in the contact respectively.

The contact stiffnesses k_n, k_t and k_r are defined in such a way that the macroscopic elastic characteristics of the particle assembly are independent of the particle size. k_n is proportional to the harmonic mean of the two particles' radii, R_1 and R_2 via the stiffness modulus, E_c. k_t and k_r are computed depending on k_n and the dimensionless tangential and rolling stiffness coefficients, α_t and α_r, respectively:

$$k_n = 2E_c \frac{R_1 R_2}{R_1 + R_2} \; ; \quad k_t = \alpha_t k_n \; ; \quad k_r = \alpha_r R_1 R_2 \, k_t \tag{4}$$

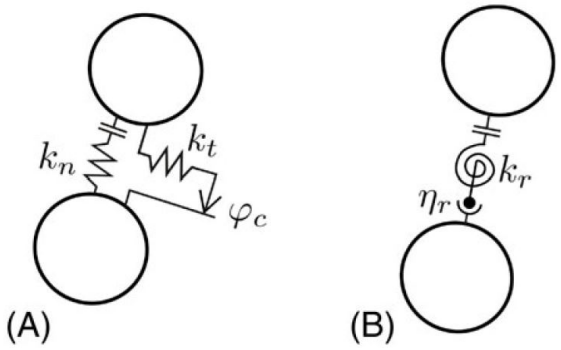

Figure 3: Inter-particle contact model with Coulomb friction (A) and rolling resistance (B).

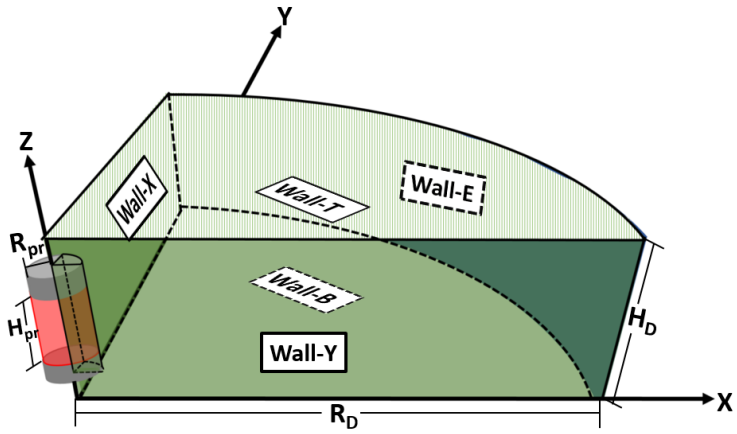

Figure 4: Schematic diagram of the pressuremeter model, the red zone represents the inflatable cell of the pressuremeter and the green zone is filled with the particles representing the soil.

3.2. Boundary conditions and probe inflation

The numerical model of the pressuremeter test has been developed with the open-source software YADE (Šmilauer et al., 2015). The geometry of the pressuremeter probe in the calibration chamber presents a rotational symmetry with respect to the vertical axis. Consequently, the size of the simulation domain could be limited to a given angular sector of the real problem in order to reduce the computational cost. However, a previous study (Hosseini-Sadrabadi, 2019) shown that the simulation domain should not be smaller than a quarter of the real problem to avoid artefact on the interaction between the granular assembly and the intruder (as a penetrometer tip or here the pressuremeter probe). Therefore, only a quarter of the domain is represented numerically as shown in Figure 4. This choice is validated in the next section by comparison with a model where the whole domain is represented. Rigid walls (walls X, Y, B, T and the cylindrical wall E as labelled in Figure 4) are used for modeling the outer boundaries of the simulation domain. Limit conditions related to the calibration chamber are reproduced by fixing the walls X, Y and E, while the bottom and top walls, B and T respectively, can translate vertically to impose the vertical stress on the granular

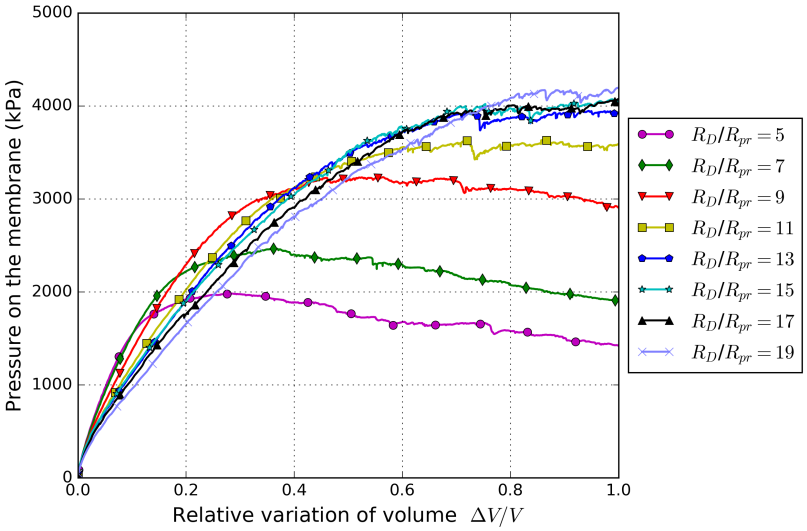

Figure 5: Simulated pressuremeter curves from a dense initial granular packing for different ratios of the radius of the simulation domain to the probe radius (R_D/R_{pr}).

assembly thanks to a closed-loop control.

The model of the pressuremeter probe is constituted of a top and a bottom cylindral parts (in grey in Figure 4) which are fixed, and a cylindrical wall (in red in Figure 4) representing the inflatable membrane of the probe. The probe's expansion is simulated by increasing the radius of this cylindrical wall up to doubling its internal volume, as for the experimental test.

Contact between soil particles and external walls is considered perfectly smooth and contact friction angle and rolling friction are set to zero. By this way the impact of the external boundaries on the simulated response is limited. For the contact between the probe and the soil, contact friction angle is also set to zero but rolling friction is kept at the same value as in the soil bulk.

Modeling a boundary value problem requires a critical choice of the size of the simulation domain. On one hand, if the size is huge, a significant number of particles is needed, which is computationally expensive; on the other hand if the size is too small the impact of virtual boundaries on the simulated response may not be negligible. This is typically the case of the radius R_D of the external cylindrical wall (Wall-E). Therefore, results of simulations of probe inflation for different values of the ratio R_D/R_{pr} (where R_{pr} is the radius of the probe) are presented in Figure 5. Simulations were performed with the parameters detailed further in the article in Table 1 (with φ_c and η_r fixed at 19° and 0.55 respectively) and from a very dense initial state of the granular assembly. It is worth saying that the effect of the ratio R_D/R_{pr} is more important in dense samples than a loose one (Wesley, 2002). Pressuremeter curves, and in particular the limit pressure p_l (i.e. the pressure reached for a doubling of the probe volume), are almost independent of the ratio R_D/R_{pr} when it is greater than 13. A ratio of 17 is considered in the following of this study.

Effect of the height of the simulation domain and of the slenderness of the probe were also investigated through the ratios H_D/H_{pr} and H_{pr}/R_{pr} respectively (where H_D is the height of the simulation domain and H_{pr} the height of the probe). Again, simulated pressuremeter curves are insensitive to these ratios for $H_D/H_{pr} \geq 3.25$ and $H_{pr}/R_{pr} \geq 2$ (For the sake of concision plots of the results are not displayed). These values are the one used in the following steps (even if experimentally the probe slenderness is 2.9).

3.3. Preparation of the granular assembly

In order to limit the number of particles and to optimize the computational cost, an adaptive discretization (Hosseini-Sadrabadi et al., 2019) of the soil medium into discrete particles is implemented. A refine discretization with a relatively low mean size of particles is performed in the neighborhood of the pressuremeter probe where deformations, at the macroscopic scale, are important and relative displacements and rearrangements of the particles, at the microscopic scale, play a key role. Then, the mean particle size increases as the distance from the probe increases, such that the coarser particles are defined close to the cylindrical wall E, where almost reversible deformations are expected, represented by an elastic response of the inter-particle contacts. The spatial rate of change of the mean particle size is limited such that the Terzaghi filter criterion holds at any point of the domain in order to avoid the migration of the finer particles close to the probe towards the outer cylindrical wall E where particles are coarser. It is worth noting that such a variable size of discretization of the medium requires a definition of the contact stiffnesses relative to the radii of the particles involved in a contact (cf. Equation 4), making the effective macroscopic properties of the granular assembly independent of the particle size.

At any point the numerical particle size distribution follows the one of the Hostun sand, except that particles smaller than 0.125 mm and greater than 0.63 mm (with respect to the real soil grading) are discarded in order to reduce the computational time. The numerical particle size distribution, scaled with respect to the mean particle size of the Hostun sand is compared with the experimental one in Figure 1.

Eventually, the soil domain is discretized using 33,000 particles with a ratio $R_{pr}/R_p = 18$ (where R_p is the local mean particle radius) at the vicinity of the probe, decreasing down to $R_{pr}/R_p = 4.8$ close to the cylindrical wall E, after the compaction process. The resulting discrete model, after compaction of the granular assembly detailed here after, is presented in Figure 6.

The granular assembly is generated from the creation of a loose cloud of particles with a relative distribution of radii as explained above. The compaction is composed of two steps as represented in Figure 7. There is an initial compaction by particle growing which is rather isotropic, followed by a vertical compression as performed experimentally. The first compaction by expanding the radius of the particles (Chareyre et al., 2002) is used to compact the assembly until reaching a relatively low mean pressure of 30 kPa (Figure 7a). During this phase the contact friction angle is tuned in order to reach the desired porosity after compaction (Figure 7b). Lower contact friction angles results in denser granular assembly. At the end of this step, the contact friction angle is changed to the nominal one (i.e.

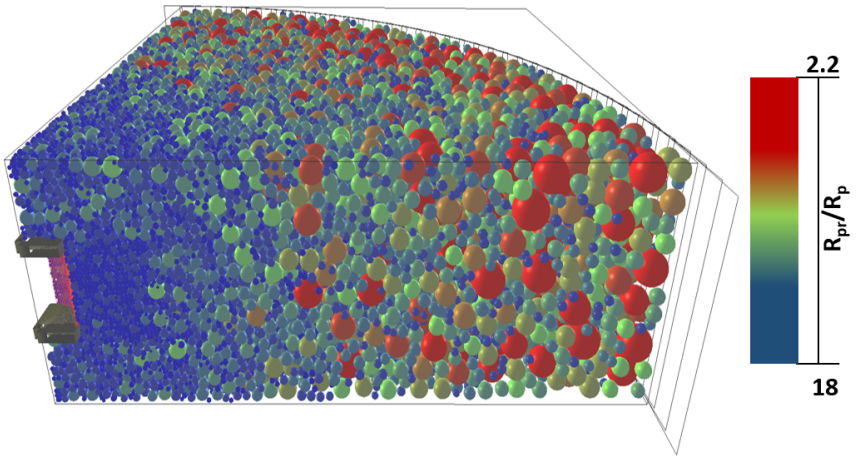

Figure 6: Discrete element model of the pressuremeter test with an adaptive size of discretization of the soil domain.

the contact friction angle used to simulate probe inflation). Experimentally there was no isotropic confining pressure applied by the calibration chamber on the sand but only a vertical stress. Therefore, the confining pressure generated by the expansion method is removed by reducing the size of the particles at a very slow rate until the mean pressure is almost nil (1 kPa), and the assembly is compressed vertically up to the desired vertical stress of 100 kPa, as imposed experimentally (Figure 7a) and until reaching an unbalanced force ratio (ratio of the mean resultant particle force to the mean contact force) less than 10^{-3} (Figure 7b). This state is considered sufficiently close to the static equilibrium and constitutes the initial state for the simulation of the probe inflation.

Two validations are presented here after regarding respectively the adaptive discretization implemented in the model and the representation of a quarter of the domain only. First, the homogeneity of the porosity of the granular assembly built with the adaptive discretization is compared with the porosity obtained from the same model, but with a constant mean value of the particle radii, such that $R_{pr}/R_p = 4$ in the whole simulation domain. Figure 8 shows the local porosity versus the dimensionless distance from the rotational axis of symmetry R/R_{pr} (where R is the radial distance from the axis of symmetry) for the two kinds of discretization. The local porosity is calculated in a given volume of investigation centered on the point of measurement. There is a similar low scattering of porosity as the distance from the probe increases for both cases. This scattering tends to be slightly more important far from the probe with the adaptive discretization as particles are coarser. This induces a stronger variability of the porosity measurement for the same size of volume of investigation. However, the homogeneity of the granular assembly made with the adaptive discretization remains satisfactory when compared to the non adaptive case.

Concerning the representativeness of considering a quarter of the domain instead of the whole one, the pressure-volume curve simulated from a quarter of the domain is compared in Figure 9 with the one simulated from the whole numerical description of the domain. In the latter case 130,000 particles where used to discretize the soil instead of

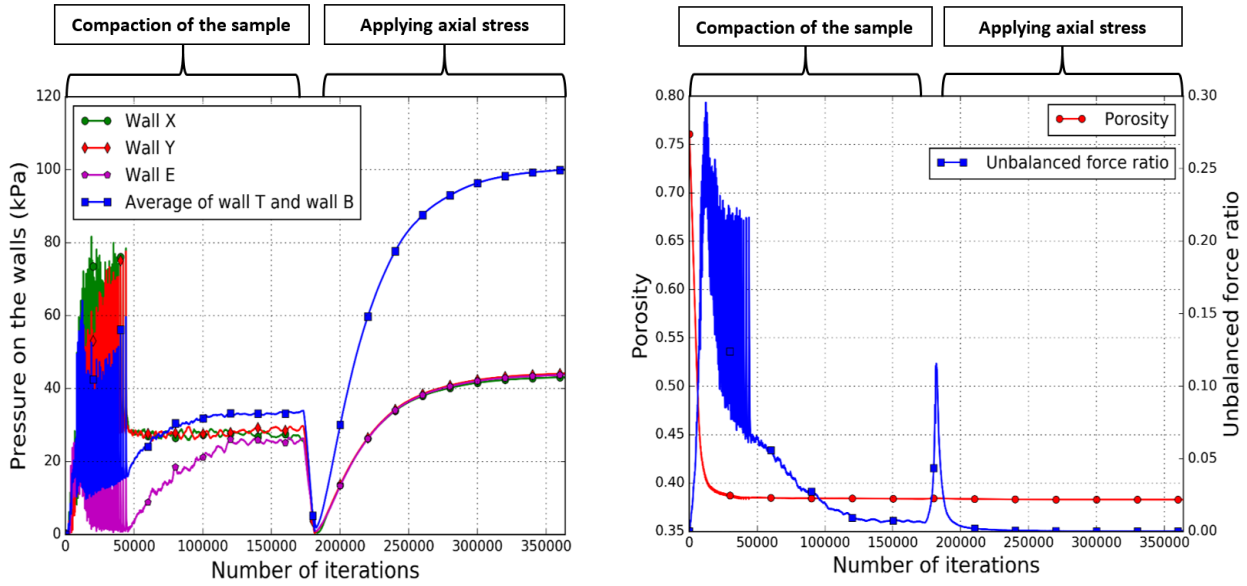

(a) (b)

Figure 7: Preparation of the granular assembly by an initial compaction of the granular assembly followed by the application of the vertical stress: pressures on the boundary wall of the simulation domain (a) and porosity and unbalanced force ratio (b).

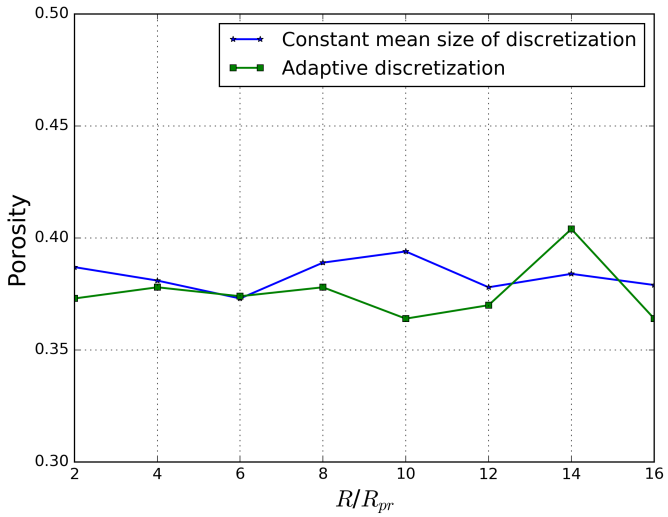

Figure 8: Comparison of the local porosity of granular assemblies built with and without the adaptive discretization technique.

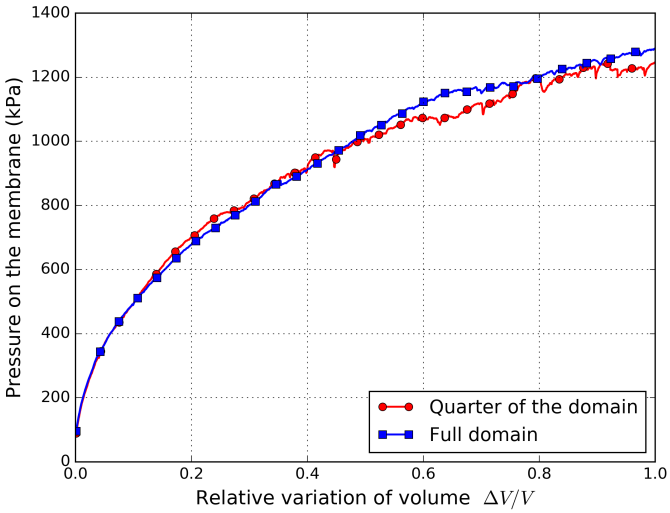

Figure 9: Comparison of pressuremeter curves simulated from the numerical representations of a quarter of the soil domain and of the full domain respectively.

33,000 particles for the representation of the quarter of the domain as shown in Figure 6. The model parameters are the same for both configurations (with φ_c and η_r fixed at 19° and 0.55 respectively, and initial porosity n_0 equal to 0.380). Both simulations give quasi identical results showing that representing a quarter only of the problem with rotational symmetry, and the associated boundary conditions, is enough to model the pressuremeter test.

4. Parametric study

In this section, the effects of the parameters of the discrete model on the simulated pressure-volume curve are investigated with the aim of defining a methodology for the calibration of the numerical model from the pressuremeter test. Both mechanical parameters related to the inter-particle interaction law and the initial density of the granular assembly are considered. Table 1 gives the values of the initial porosity n_0 and the contact parameters used for this parametric study.

For the sake of conciseness, the parametric study focuses on the role played by the "plastic" contact parameters (i.e. the contact friction angle φ_c and the rolling friction coefficient η_r) and the initial porosity. Elastic contact parameters are chosen here sufficiently high to approach the limit of rigid particles (Roux and Combe, 2010; Roux and

Table 1: Contact parameters and initial porosity used for the parametric study.

	E_c (MPa)	α_t	α_r	φ_c (deg)	η_r	n_0
Case 1	500	0.3	5	10-40	0.55	0.368
Case 2	500	0.3	5	19	0.01-0.9	0.352
Case 3	500	0.3	5	19	0.55	0.329-0.401

Chevoir, 2005) and avoid by this way an interdependence between local elastic stiffnesses and macroscopic plastic properties of the granular assembly (Aboul Hosn et al., 2017; Zhao et al., 2018). In these conditions, the impact of the elastic contact parameters on the pressure-volume curve is rather limited and is not displayed here. Note that the value of E_c could be tuned to reproduce the slope of the pressure-volume curve at small deformations as long as it stays close to the rigid particle limit. Initial slope of the pressure-volume curve could also be affected by the initial connectivity of the granular assembly depending on its preparation methodology (Sibille et al., 2021).

4.1. Sliding and rolling friction

Contact friction angle, φ_c, and rolling friction, η_r, representing the dry friction at contact and the shape of the particles respectively, are considered as the primary parameters of the model that control the macroscopic plastic response of the granular assembly. Their impact on the pressure-volume curve is investigated by performing simulations of probe inflation with the parameters identified as "Case 1" in Table 1, to test values of φ_c ranging from 10° to 40°, and as "Case 2" to test values of η_r from 0.01 to 0.9.

Besides, contrary to the physical pressuremeter test, where the volumetric deformation of the soil cannot be measured during the probe inflation, the discrete numerical model provides the access to this information. Hence, the mean porosity of the granular assembly in the direct vicinity of the probe is calculated in a 3D window of investigation with the same height as the probe with a length and width equal to 1.6 R_{pr}.

Figures 10 and 11 present the pressure-volume curves and the changes in porosity near the probe for the parametric studies on φ_c and η_r respectively. The contact friction angle impacts both the limit pressure and the volumetric deformation of soil, with an important increase in the limit pressure from 600 kPa (for $\varphi_c = 10°$) to 7000 kPa (for φ_c =40°) (Figure 10a) and of the soil dilatancy (Figure 10b) with φ_c. The rolling friction affects the limit pressure similarly to φ_c, with a higher limit pressure (from 800 kPa to 3300 kPa) for a larger rolling friction (from 0.01 to 0.5). However a saturation is observed for $\eta_r > 0.5$ where the limit pressure is independent of η_r beyond this threshold (Figure 11a). Contrary to φ_c, the volumetric response of the soil depends only weakly on η_r (Figure 11b). These results are in agreement with the effects of the rolling friction on the simulated responses to drained triaxial compressions as described for instance in Aboul Hosn et al. (2017): the peak shear strength increases with η_r but then tends to

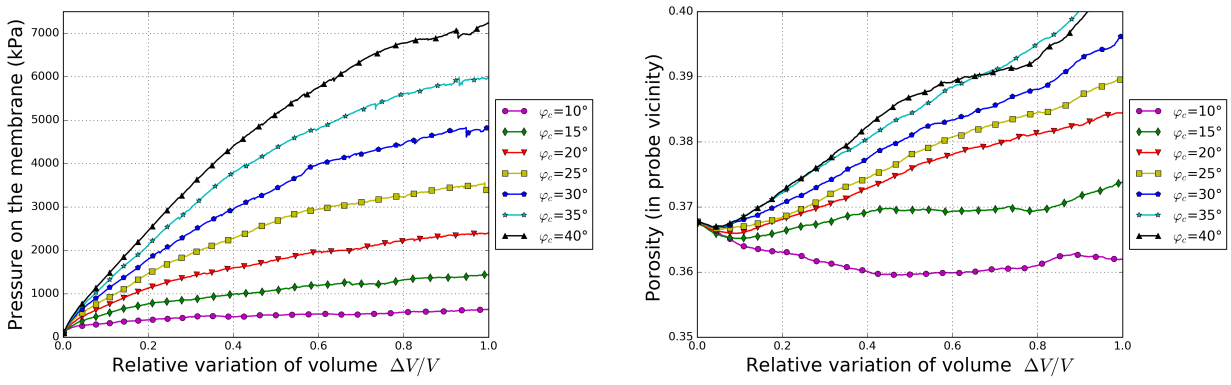

(a) (b)

Figure 10: Pressure-volume curves (a) and porosity variations nearby the probe (b) simulated for different values of the contact friction angle (Case 1 in Table 1).

stabilizes for values of η_r above 0.3 to 0.7. In addition, a wider range of volumetric responses (dilatancy) is reachable by changing φ_c rather than η_r.

4.2. Initial porosity

The constitutive behaviour of a "real" soil is strongly dependent on its initial density, affecting directly the volumetric deformation and the maximum shear strength. Thus, the initial density of the granular assembly is an important parameter to investigate and probe inflation has been simulated with the parameters of the "Case 3" in Table 1, considering a range of initial porosities, n_0, from 0.329 to 0.401. Figure 12 shows a significant effect of the initial porosity on the limit pressure and the volumetric deformation. As the initial porosity decreases, the granular assembly is denser and present a higher resistance to the probe inflation together with a more dilatant response.

To resume, the contact friction angle and the initial porosity affect similarly the simulated soil response to the probe inflation, affecting significantly both the pressure-volume curve (with among others the limit pressure) and the volumetric deformation. Consequently, there is no independent relationship between the model response to the probe inflation and n_0 or φ_c. Nevertheless, the volumetric response could be assumed as independent of the rolling friction coefficient η_r (even it is not totally true), in order to isolate the effect of η_r from n_0 and φ_c. However, there is still an interplay between η_r, n_0 and φ_c with respect to the limit pressure and the pressure-volume curve.

5. Initial state and calibration of the discrete model from the pressuremeter test

The parametric study showed that the simulated response to the probe inflation depends mainly on the plastic contact parameters and the initial porosity of the granular assembly. The contact elastic parameters are considered as secondary parameters, and their effect can be significantly reduced as long as the chosen values are close to the rigid

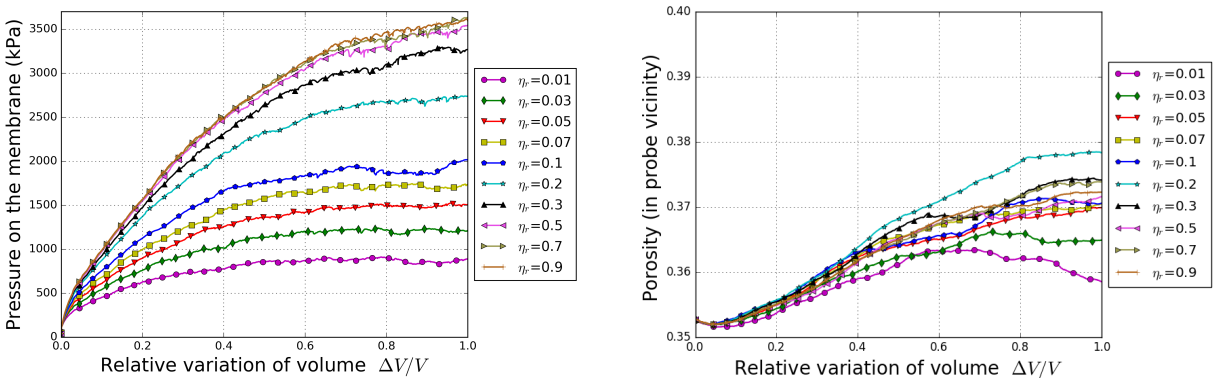

(a) (b)

Figure 11: Pressure-volume curves (a) and porosity variations nearby the probe (b) simulated for different values of the rolling friction coefficient (Case 2 in Table 1).

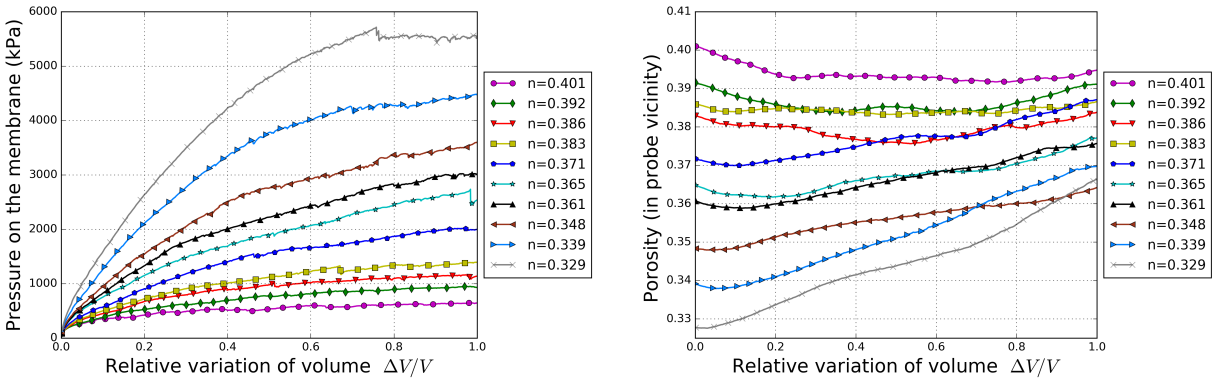

(a) (b)

Figure 12: Pressure-volume curves (a) and porosity variations nearby the probe (b) simulated for different initial porosities.

particle limit. Therefore, the calibration process can be limited to plastic parameters: contact friction angle, φc, and rolling friction coefficient, η_r, once the soil's initial porosity n_0 is fixed.

However, as there is no uncoupled relation between the characteristics of the pressure-volume curve and each of these three parameters, there is no possibility to calibrate both φ_c and η_r from a pressuremeter test only.

5.1. Choice of the initial porosity

The initial porosity of the model could be fixed independently of the pressure-volume curve by following one of the following three approaches (Sibille et al., 2019):

i The first approach is to assign the porosity of the real soil to the numerical granular packing. This solution is quite straightforward to implement but it assumes that for a given initial porosity the real soil and the numerical packing should undergo similar volumetric deformations, which may not holds if the grain shape is different;

ii The second approach is to assign the relative density of the real soil (here $D_r = 83\%$) to the numerical packing. This option can be implement by considering the maximum and minimum void ratios achieved in the numerical assembly. Again, this approach assumes that the numerical assemblies at minimum and maximum relative densities simulate the same mechanical responses as the real soil at the same minimum and maximum relative densities.

iii The third approach consists of adjusting the initial porosity of the numerical sample in a way to reproduce the same volumetric deformation of the real soil. This actually depends on the difference between the initial porosity and the one at the critical state for the numerical model and the real soil respectively

Regarding the calibration of the discrete model from the pressuremeter test, the third option cannot be considered as the test does not provide any information about the soil's volumetric response. Consequently, the first and the second options only will be considered as two different scenarios. The determination of the relative density for the numerical model requires to define minimum and maximum void ratios, e_{max} and e_{min} (or porosities). e_{min} is obtained after the compaction of the granular assembly with $\varphi_c = 0$, whereas e_{max} is reached by prohibiting the tangential sliding at contacts.

5.2. Rolling friction coefficient, η_r, calibration

Aboul Hosn et al. (2017) has shown that the shear strength at critical state depends only on the rolling friction coefficient (if $\varphi_c \geq 15°$). Consequently, η_r can be calibrated independently of the other parameters if the information about the critical state is available. Such information cannot be deduced from the pressuremeter test and we made the choice to take advantage of the knowledge of the shear strength at large deformation for the Hostun sand (deduced from triaxial compressions) and the corresponding value of the rolling friction coefficient. Hence from previous studies, a first value of $\eta_r = 0.55$ has been determined from triaxial compressions performed on a dense Hostun sand (Sibille et al., 2019). Then, thanks to a refine assessment of the shear strength at large deformation based on triaxial

Table 2: Parameters of the discrete model deduced from the calibration from the experimental pressuremeter test.

Parameter set	Approach	n	η_r	φ_c (deg)	E_c (MPa)	α_t	α_r
1	Same absolute density	0.405	0.55	23.5	500	0.3	5
2	Same relative density	0.359	0.55	12.0	500	0.3	5
3	Same absolute density	0.405	0.25	26.5	500	0.3	5
4	Same relative density	0.353	0.25	10.5	500	0.3	5
5	Same absolute density	0.405	0.10	43.0	500	0.3	5
6	Same relative density	0.348	0.10	10.5	500	0.3	5

compressions on both dense and loose Hostun sand, the rolling friction coefficient has been reevaluated at $\eta_r = 0.25$ (Sibille et al., 2021). Both values of η_r are intended to be representative of Hostun sand regardless its initial density. Nevertheless, the second value can be considered as a more representative calibration.

These two values of η_r are considered in this study in addition to another one, $\eta_r = 0.1$, chosen arbitrarily to widen the range of investigation. For every value of η_r the two different approaches of identifying the initial porosity will be used. Therefore, six different parameter sets have been identified, as detailed in Table 2. For the parameter sets with an initial numerical relative density identical to the real one, the minimum and maximum void ratios of the numerical assemblies have to be calculated for each value of η_r as they may depends on the latter, in particular the looser state (e_{max}) which is the less stable one. Table 3 shows the different maximum and minimum void ratios (or porosities) for the different values of η_r and the respective void ratios (or porosities) corresponding to a relative density of 83%.

5.3. Contact friction angle, φ_c, calibration

After defining the rolling friction coefficient, the only parameter to be calibrated is the contact friction angle φ_c. For each parameter set, different values of contact friction angle, φ_c, are tested using the pressuremeter model. The pressure-volume curves simulated with these different values of φ_c are compared visually with the experimental curve to identify which value can best fit the experimental response. This parameter has a direct influence on the plastic part of the response and much less on the pseudo-elastic phase ($\Delta V/V < 0.2$) which is mainly controlled by the elastic contact parameters and the initial state of the granular assembly. Therefore, the choice of φ_c is mainly based on the comparison of the plastic part of the pressure-volume curves (at large change of the probe volume). Table 2 shows the values of the contact friction angle obtained for each parameter set.

5.4. Results and discussion

The resulting calibrations are presented in Figure 13 according to each parameter set and compared with the experimental pressure-volume curve. The corresponding parameters of the models deduced from these calibrations are given in Table 2.

Table 3: Maximum and minimum void ratios (porosities) obtained for different values of η_r and the respective void ratios (porosities) corresponding to a relative density of 83%, as for the sand used for the pressuremeter test.

η_r	n_{max}	n_{min}	e_{max}	e_{min}	e	n
0.55	0.475	0.329	0.904	0.490	0.560	0.359
0.25	0.456	0.329	0.838	0.490	0.549	0.354
0.1	0.437	0.329	0.776	0.490	0.538	0.350

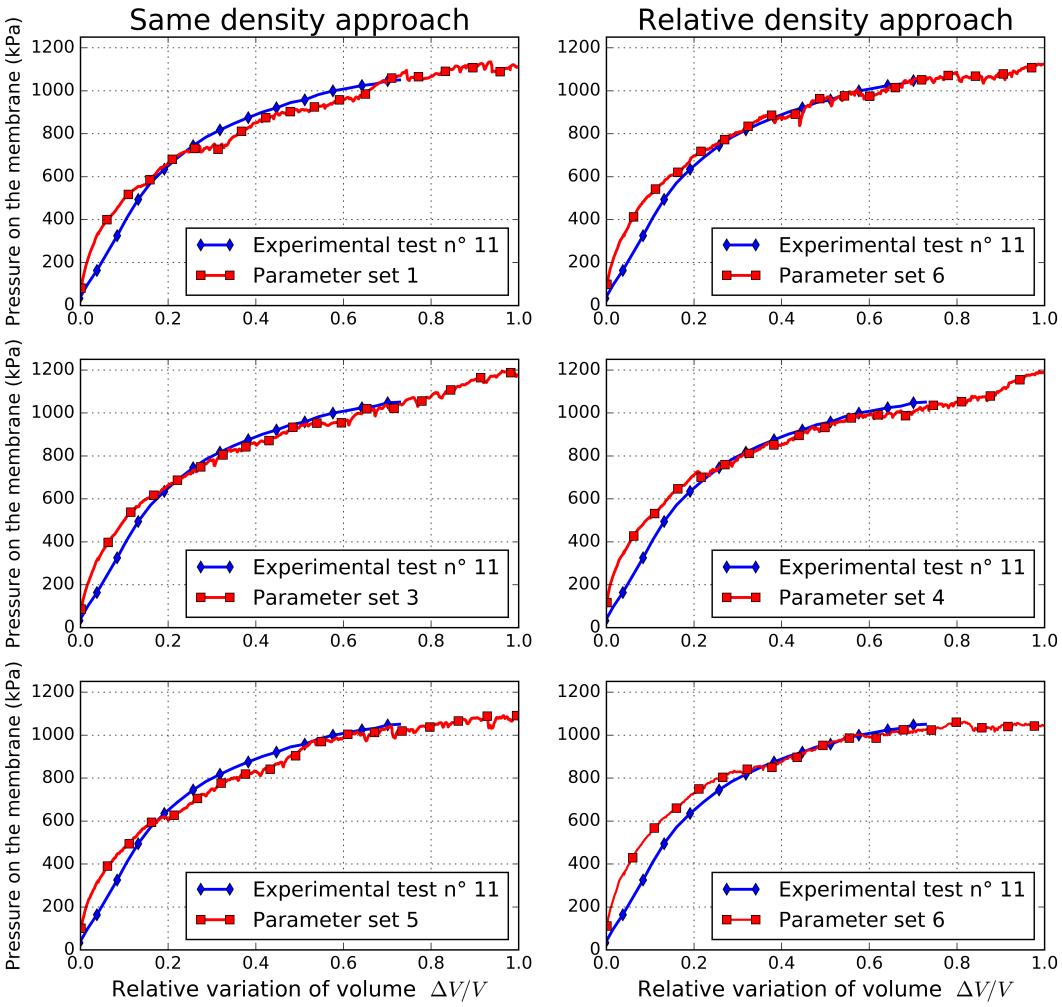

Figure 13: Simulations of the pressuremeter test according to the six different parameter sets of calibration compared to the experimental text results.

For all the parameter sets the limit pressure is correctly reproduced by the model. Nevertheless, in all the cases the model slightly overestimates the stiffness (i.e. the slope of the pressure-volume curve) in the pseudo-elastic phase for $\Delta V/V < 0.2$. This could be fitted, at least partially, by tuning the contact stiffness E_c. However, the experimental curve presents itself in this pseudo-elastic phase a shape not strictly convex (the slope of the pressure-volume curve is not strictly decreasing with the inflation of the probe) which may be attributed to a slight experimental drawback. The presence of probe during the sand pluviation may affect the density of the sand in the direct vicinity of the probe and impact by this way the pressure-volume curve at the beginning of the probe inflation (Mokrani, 1991). Consequently, there was no clear reason to attempt to fit more closely the experimental curve in this phase.

In all cases, these results show clearly that a unique set of parameters of the discrete model cannot be identified from data of a pressuremeter test. Fahey and Carter (1993) and Biarez et al. (1998) reached the same conclusion concerning the calibration of elasto-plastic constitutive relations since the latter were able to describe a given experimental pressure-volume curve with different mechanical input parameters. Nevertheless, the parameter sets 2, 4 and 6 leads to the identification of very low contact friction angles, lower than 15°. Such weak values may not be representative of the contact of silica particles (Kawamoto et al., 2018) and may constitute a drawback for the discrete model itself (Aboul Hosn et al., 2017). Therefore, parameter sets 1, 3 and 5 should a priori be preferred to parameter sets 2, 4 and 6.

Furthermore, the coefficient of earth pressure at rest, K_0, was deduced experimentally from measurements of the vertical, σ_v, and horizontal, σ_h, stresses with "Glötzl" stress gauges. K_0 was equal to 0.30 once the soil sample is built and subjected to the vertical stress (i.e. before the inflation of the probe). In the simulations, this coefficient is determined with σ_h calculated as the average stress on the vertical walls (Walls X, Y and E) and σ_v as the average stress on the bottom and top wall (walls B and T). After the application of the vertical stress, $K_0 = 0.39$, 0.43, and 0.51 for the parameter sets 1, 3, and 5 respectively and $K_0 = 0.52$, 0.53, and 0.55 for parameter sets 2, 4 and 6. These results show that parameter sets 1, 3 and 5 lead also to earth pressure coefficients at rest closer to the value obtained experimentally (the closest being the parameter set 1).

6. Validation from laboratory tests

Validation tests, consisting of different kinds of loadings than the one induced by the pressuremeter test, are considered to assess the relevance of the sets of parameters identified previously and to possibly discriminate them. For that purpose, three different loading paths performed with a true triaxial apparatus on cubical samples of Hostun sand are considered. The side length of the sand samples is initially 10 cm and they are compacted in a dense state ($D_r = 100\%$). Compaction and loading are all performed in dry condition. The first loading path is a monotonous drained axisymmetric triaxial compression under a confining pressure of 200 kPa. The second kind of path is a cyclic stress proportional loading with a really 3D stress state due to the proportionality fixed between the three principal stresses. Finally, the third loading is a circular stress path in the deviatoric stress plane. This loading path was used as

a reference path to benchmark the prediction ability of phenomenological constitutive relations during the Cleveland Workshop in 1987 (Saada and Bianchini, 1988). For this loading, the mean pressure and deviatoric stress are kept constant while the Lode angle is changed continuously. First and third tests were performed by Lanier and Zitouni (1988), and second test by Zitouni (1988).

These loading cases constitute homogeneous problems, contrary to the model of the pressuremeter test which is a boundary value problem with heterogeneous fields of strains and stresses. Consequently, these 3 triaxial problems are modeled with a parallelepipedic periodic cell including 10 000 particles. The particle size distribution is identical to the one used for the pressuremeter model (Figure 1). Besides, the initial relative density of the sand samples used for these triaxial tests is higher than the relative density of the sand used for the pressuremeter test ($D_r = 83\%$). Consequently, for the simulations of the validation tests, the mechanical parameters of the contact law are of course the one identified in Table 2, but the initial porosity of the numerical samples is chosen in order to be consistent with the approach applied for the identification of the parameters. Hence, it is either the same porosity as the one of the sand sample in the true triaxial apparatus ($n = 0.385$), or the same relative density $D_r = 100\%$. Therefore, the absolute value of the initial numerical porosity is different from the one indicated in Table 2 relative to the pressuremeter tests.

6.1. Axisymmetric triaxial compression

Simulated responses to the triaxial compression are compared with the experimental results plotted with a thick magenta line in Figure 14. The experimental test includes one cycle of unloading-reloading which is not simulated (prediction ability of the model with respect to cyclic loadings is investigated with the next validation case). Each simulation is performed with a set of mechanical parameters calibrated according to one of the six parameter sets respectively, as displayed in Table 2. Parameter sets defined with the same approach for the determination of the initial sample porosity (either absolute density, or relative density identical to the physical sand samples) are grouped together in Figure 14.

Concerning the "absolute density approach" (odd parameter sets), the shear strength at large deformation decreases from parameter set 1 to parameter set 5. This is in agreement with the fact that the critical shear strength depends only on the rolling friction (if the contact friction angle is high enough) (Aboul Hosn et al., 2017) since the rolling friction, η_r descreases from parameter set 1 to 5. Conversely, the dilatant behaviour, strongly dependent on the contact friction angle, is more pronounced for parameter set 5 where the contact friction angle is the highest , than for parameter set 1 with the lowest contact friction angle (among parameter sets 1, 3 and 5).

Concerning the "relative density approach" (even parameter sets), the shear strength at large deformation is only weakly depending on the rolling friction. Moreover it is apparently not in agreement with the shear strength at large deformation simulated with the absolute density approach. For instance, the rolling friction for parameter sets 1 and 2 ($\eta_r = 0.55$) is the same, thus the critical shear strength should be the same for these two parameter sets.

However, the values of the contact friction angles calibrated with the relative density approach are all very low (φ_c ranges from 10.5 to 12 deg). Such values may be not representative of the friction properties between two silica sand

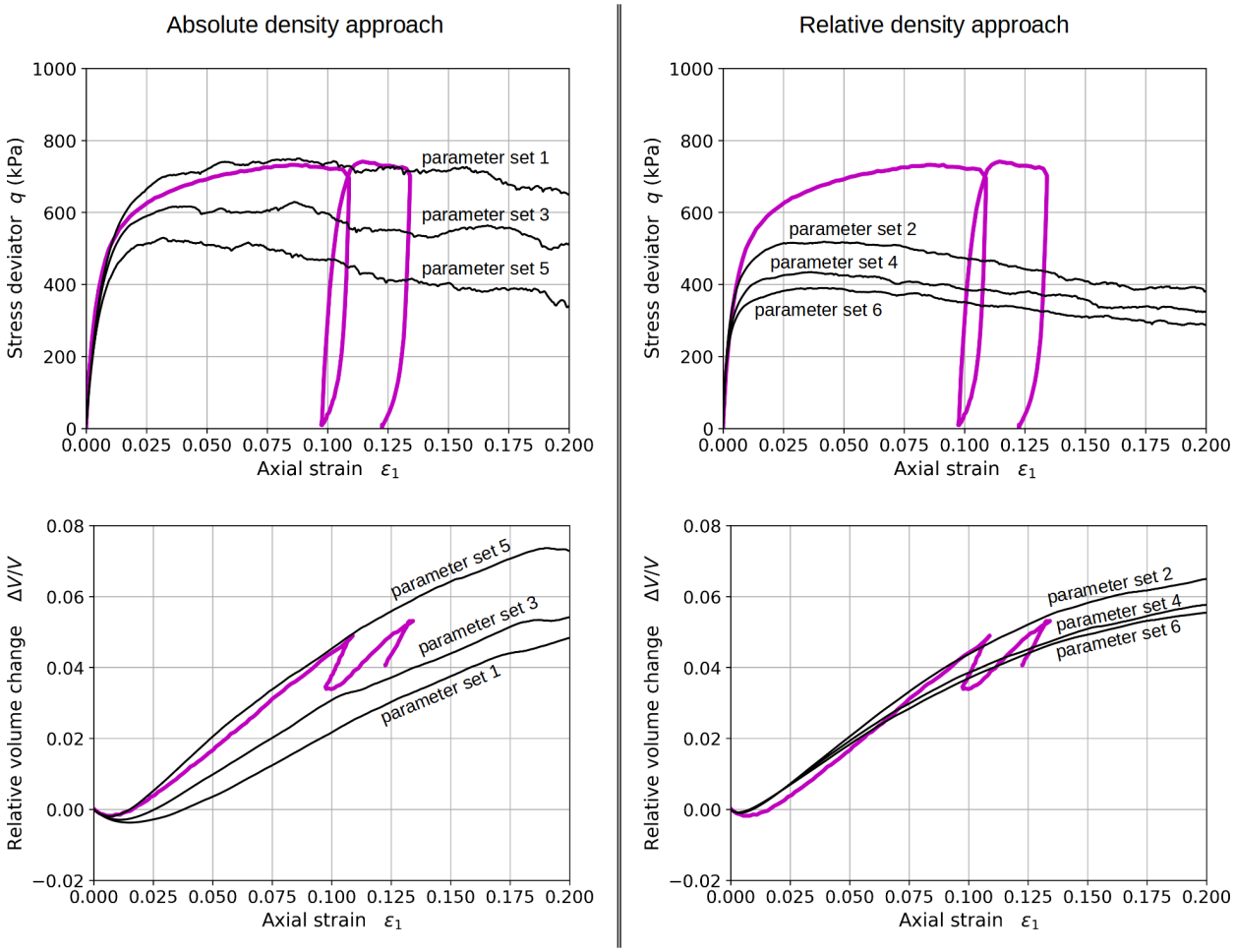

Figure 14: Axisymmetric triaxial compression on dense Hostun sand: comparaison of the experimental results with thick magenta (or grey in black and white printings) line and simulated predictions with thin black lines.

Table 4: Final set of parameters for the pressuremeter model

Approach	n	η_r	φ_c (deg)	E_c (MPa)	α_t	α_r
Same absolute density	0.405	0.55	23.5	500	0.3	5

grains (Kawamoto et al., 2018) and below the threshold of 15 deg identified by Aboul Hosn et al. (2017) to avoid an interplay between the rolling friction and the contract friction angle on the critical shear strength. Consequently, the parameter sets identified with the relative density approach could be discarded for this reason. The dilatant behaviour is almost the same for parameter sets 2, 4 and 6 since the contact friction angles and the initial porosities are very close for these sets of parameters.

Finally, all the simulated responses to the drained compression are consistent with the values of the respective sets of parameters used. However, only the parameter set 1 gives a satisfying prediction of the constitutive response to this loading path, even if the dilatancy is a little underestimated. Consequently, parameter sets 1 only is considered for the next validation cases.

To sum up, the final mechanical parameters of the model and its initial density state (parameter set 1) have been defined as follows:

- The initial porosity was assigned equal to the porosity of the real soil;
- The three elastic parameters E_c, α_t and α_r were presumed with sufficiently high values to avoid the interdependence between local elastic stiffnesses and macroscopic plastic properties;
- The rolling friction coefficient, η_r, was calibrated from a rough estimation of the shear strength of Hostun sand at the critical state based on a triaxial drained compression (Sibille et al., 2019);
- The contact friction angle, φ_c, was calibrated by tuning this value in the pressuremeter model until the simulated pressure-volume curve best fits the experimental one, in particular for a large inflation of the probe ($\Delta V/V > 0.2$).

Table 4 summarizes the validated set of parameters of the pressuremeter model.

6.2. Cyclic stress proportional loading paths

For stress proportional loading paths the intermediate principal stress σ_2 is fixed with respect to the major and minor principal stresses, σ_1 and σ_3 respectively, thanks to the parameter b kept constant for a given loading:

$$b = \frac{\sigma_2 - \sigma_3}{\sigma_1 - \sigma_3} = cst. \tag{5}$$

For the test considered here $b = 2/3$ and the mean pressure is kept constant and equal to 500 kPa. In addition, loading/unloading cycles are performed by imposing the amplitude of the strain in direction 1 such that $\Delta\varepsilon_1 = 4.9\%$,

except for the first cycle with a larger amplitude. Experimental results are compared with the response simulated according to the parameter set 1 in Figure 15. The stress-strain response is rather well predicted by the model, but the volumetric deformations are slightly overestimated. In particular, for the initial compression, strain localization occurred experimentally quite early (around $\varepsilon_1 = 2.5$ to 3 %) (Zitouni, 1988) deviating the measured soil response from what should be the constitutive response. Consequently, experimental response cannot be compared rigorously with the predicted one for the initial compression, beyond this state. In all cases, it can be considered as a good performance for a model calibration performed on a single monotonous tests (conventional constitutive models dedicated to cyclic soil responses are usually calibrated from cyclic tests).

6.3. Circular stress path

The circular stress path is performed by keeping constant the mean pressure p, equal to 500 kPa, and the second stress invariant $I_{2\sigma}$, equal to 420 kPa (representing the intensity of the deviatoric stress), while the Lode angle φ_σ is progressively inscreased from -120 deg to +600 deg ($\varphi_\sigma = 0$ correspond to the direction of the axis s_1 which is the projection of the σ_1 axis in the deviatoric stress plane). Consequently, the mechanical state of the sand sample is controlled by imposing the stress state such that:

$$\begin{aligned} \sigma_1 &= p + \sqrt{2/3}\, I_{2\sigma} \cos(\varphi_\sigma) \\ \sigma_2 &= p + \sqrt{2/3}\, I_{2\sigma} \cos(\varphi_\sigma - 120^o) \\ \sigma_3 &= p + \sqrt{2/3}\, I_{2\sigma} \cos(\varphi_\sigma + 120^o) \end{aligned} \tag{6}$$

The initial state of the circular stress path is reached by realizing first an isotropic compression up to 500 kPa, followed by a compression at constant mean pressure in direction '3' (i.e. such that $\varphi_\sigma = -120$ deg) until reaching $I_{2\sigma} = 420$ kPa.

The response predicted by the model (parameter set 1) is compared with the experimental one in Figure 16. The strain response path is displayed as its projection in the deviatoric strain plane from one hand, and as the relative volume change (representing the component of the strain path out of the deviatoric strain path) on the other hand. Concerning the initial compression at constant mean pressure along direction '3', the model describes a purely deviatoric deformation (visible in the deviatoric strain plane) whereas experimentally both deviatoric and volumetric deformations have been observed. Then, regarding the circular stress path itself, the model globally underestimates the amplitude of the deformations both deviatoric and volumetric, but gives an acceptable and realistic prediction of the sand response. It is worth noting that the shift in the volumetric strain at the end of the circular path (i.e. for $\varphi_\sigma = 600$ deg) results only partially from the circular loading, the other part coming from the initial compression. Consequently, the relative shift in the volumetric strain between the experimental and the simulated results due to the circular loading is 38%.

Furthermore, it is important to keep in mind that conventional elasto-plastic constitutive relations are not able to describe a realistic soil response (even qualitatively) for this kind of loading path (because the plastic mechanisms in

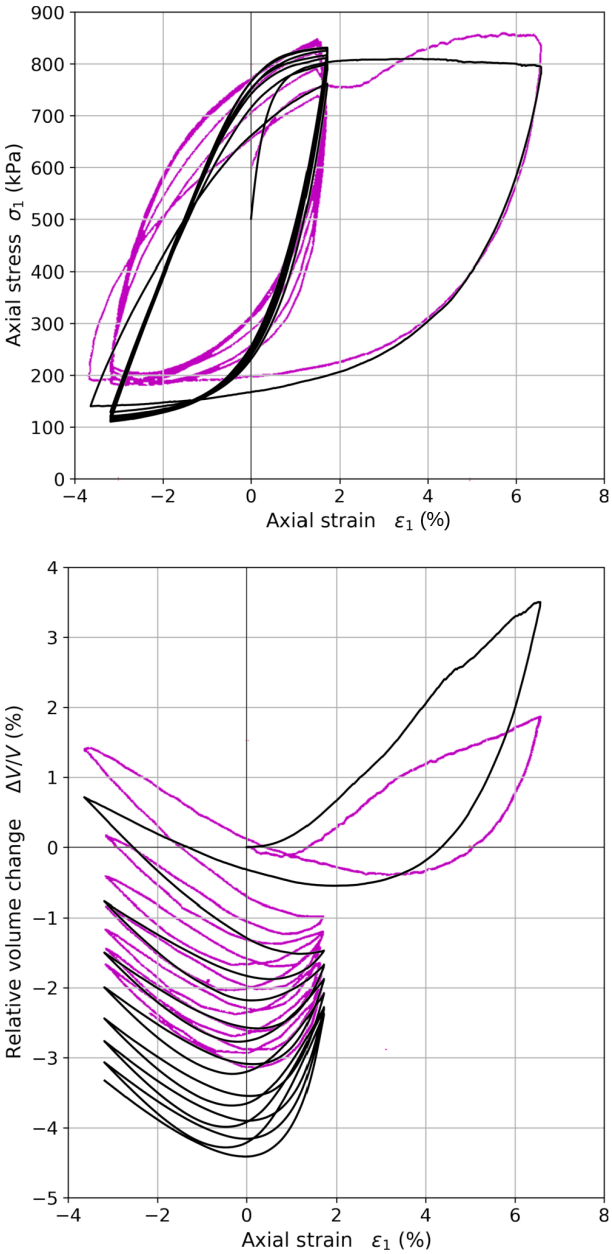

Figure 15: Cyclic proportional stress loading path at constant mean pressure: comparaison of the experimental results with magenta (or grey in black and white printings) line and simulated prediction with black line.

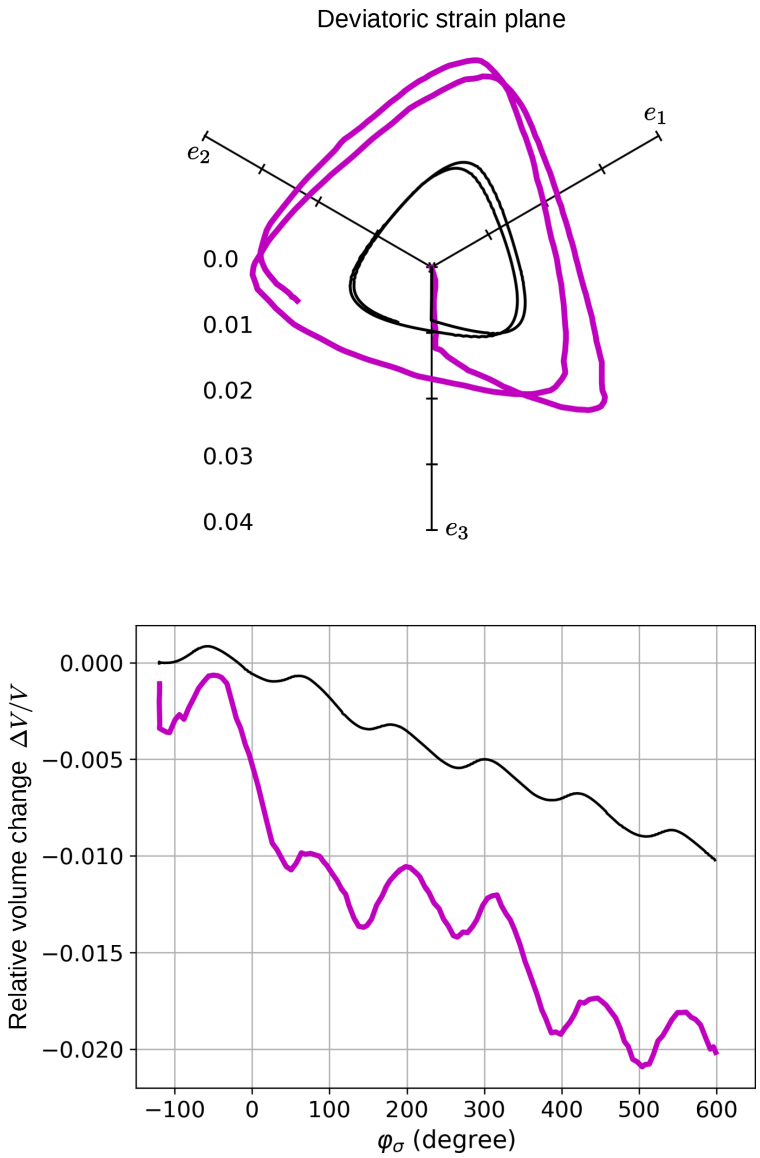

Figure 16: Strain response to a circular stress loading path in the deviatoric stress plane: comparaison of the experimental results with thick magenta (or grey in black and white printings) line and simulated predictions with thin black line.

such relations are usually related to changes in the mean pressure, or of the deviatoric stress which do not occur along the circular stress path) (Saada and Bianchini, 1988). Only advanced incrementally non-linear constitutive relations have shown their ability to produce a good prediction of the soil response in these conditions (Darve and Dendani, 1988). However these models involve an important number of parameters requiring several axisymmetric triaxial tests in compression and extension to be calibrated. Therefore, the prediction of the discrete model is here relatively good compared to the amount of experimental data necessary to calibrate it (a single pressuremeter test and the knowledge of the mobilized internal friction angle at the critical state).

7. Conclusion

A discrete numerical model of pressuremeter test has been developed. To limit the computational cost the model takes advantage of the rotational symmetry of the problem by representing numerically only one quarter of the whole domain. Morevover, the discretization of the soil into discrete particles is made dependent on the distance to the probe of the pressuremeter. In the vicinity of the probe, where important soil deformations, or even the soil failure, are expected a refine discretization is performed by representing the soil with relatively small (and numerous) discrete particles. Further from the probe, the relative mean diameters of the particles is gradually increased since particle rearrangement is less important. Hence, relatively coarse (and few) particles are enough to describe reversible deformations. By this way, the number of particles involved in the model is reduced.

The simulation of the pressuremeter test shows that the volumetric response of the soil close to the probe is rather independent (but not totally) of the rolling friction between particles. Besides, there is a cross dependency of the soil response, and in particular the limit pressure, on the contact friction angle, the rolling friction and the initial soil porosity. In other words, essentially because the dilatancy of the soil is not a measurable data from a pressuremeter test, the number of typical soil properties provided by this field test is lower than the number of model parameters. Consequently, the mechanical parameters of the discrete model and the initial density of the granular assembly cannot be identified separately from a pressure-volume curve coming from a pressuremeter test only. This conclusion is in agreement with previous studies about the calibration of elasto-plastic constitutive relations from the pressuremeter tests.

The suggested calibration methodology requires an a priori assessment of the critical shear strength of the considered soil. In addition, different parameter sets have been investigated by assigning either the initial porosity of the model, or its initial relative density, equal respectively to the initial soil porosity, or to the initial relative density of the soil. Following these different strategies, the discrete model has been calibrated from a pressuremeter test performed on Hostun sand. Then, a validation step was performed by simulating different triaxial loading paths (asymmetric and truly triaxial paths, monotonous and cyclic paths) for comparison with the experimental responses of the Hostun sand measured from triaxial loading devices. The model calibrated by assuming the initial numerical porosity identical to the initial soil porosity leads to a rather good prediction of the Hostun sand responses on the validation triaxial path.

These predictions are quite similar to what can be expected with a model calibrated from an axsymmetric triaxial compression. However the calibration relies only partially on the pressuremeter test, the assessment of the critical shear strength may either be empirical or require a specific test in itself.

References

References

Aboul Hosn, R., Sibille, L., Benahmed, N., Chareyre, B., 2017. Discrete numerical modeling of loose soil with spherical particles and interparticle rolling friction. Granular matter 19, 4.

Bahar, R., 1992. Analyse numérique de l'essai pressiométrique: application à l'identification de paramètres de comportement des sols. Ph.D. thesis. Ecully, Ecole centrale de Lyon.

Bardet, J., 1994. Numerical simulations of the incremental responses of idealized granular materials. International Journal of Plasticity 10, 879–908.

Biarez, J., Gambin, M., Gomes-Correia, A., Flavigny, E., Branque, D., 1998. Using pressuremeter to obtain parameters to elastic-plastic models for sands, in: Geotechnical site characterization, pp. 747–752.

Boubanga, A., 1990. Identification de paramètres de comportement des sols à partir de l'essai pressiométrique. Ph.D. thesis. Thèse de doctorat.

Butlanska, J., Arroyo, M., Gens, A., O'Sullivan, C., 2014. Multi-scale analysis of cone penetration test (cpt) in a virtual calibration chamber. Canadian Geotechnical Journal 51, 51–66. doi:10.1139/cgj-2012-0476.

Chareyre, B., Briançon, L., Villard, P., 2002. Theoretical versus experimental modeling of the anchorage capacity of geotextiles in trenches. Geosynthetics International 9, 97–123. doi:10.1680/gein.9.0212.

Ciantia, M., Arroyo, M., Calvetti, F., Gens, A., 2016. A numerical investigation of the incremental behavior of crushable granular soils. International Journal for Numerical and Analytical Methods in Geomechanics 40, 1773–1798. doi:https://doi.org/10.1002/nag.2503.

Cundall, P.A., Strack, O.D., 1979. A discrete numerical model for granular assemblies. geotechnique 29, 47–65.

Darve, F., Dendani, H., 1988. An incrementally non-linear constitutive relation and its predictions, in: Saada, A., Bianchini, G. (Eds.), Constitutive equations for granular non-cohesive soils - Proceedings of the international workshop on constitutive equations for granular non-cohesive soils, Balkema, Rotterdam, 22-24 July 1987, Cleveland. pp. 237–254.

Fahey, M., Carter, J.P., 1993. A finite element study of the pressuremeter test in sand using a nonlinear elastic plastic model. Canadian Geotechnical Journal 30, 348–362.

Flavigny, E., Desrues, J., B., P., 1990. Le sable d'hostun rf. Revue Française de géotechnique , 67–70.

Geng, Y., 2010. Discrete element modelling of cavity expansion in granular materials. Ph.D. thesis. University of Nottingham Nottingham, UK.

Hosseini-Sadrabadi, H., 2019. Identificiation in-situ des sols liquéfiables par pénétromètre statique cyclique : modélisations physiques et numériques. Ph.D. thesis. Université Grenoble Alpes. Grenoble, France.

Hosseini-Sadrabadi, H., Celeste, F., Chareyre, B., Dano, C., Sibille, L., Riegel, P., 2019. Interpretation of a cyclic cone penetration test (cpt) under saturated conditions: numerical and experimental approaches., in: Proceedings of the XVII ECSMGE-2019 Geotechnical Engineering foundation of the future. doi:10.32075/17ECSMGE-2019-0260.

Huang, A.B., Ma, M.Y., 1994. An analytical study of cone penetration tests in granular material. Canadian Geotechnical Journal 31, 91–103.

Iwashita, K., Oda, M., 2000. Micro-deformation mechanism of shear banding process based on modified distinct element method. Powder Technology 109, 192–205.

Kawamoto, R., Ando, E., Viggiani, C., Andrade, J., 2018. All you need is shape: Predicting shear banding in sand with ls-dem. Journal of the Mechanics and Physics of Solids 111, 375–392. doi:10.1016/j.jmps.2017.10.003.

Lanier, J., Zitouni, Z., 1988. Development of a data base using the grenoble true triaxial apparatus, in: Saada, A., Bianchini, G. (Eds.), Constitutive equations for granular non-cohesive soils - Proceedings of the international workshop on constitutive equations for granular non-cohesive soils, Balkema, Rotterdam, 22-24 July 1987, Cleveland. pp. 47–58.

Li, L., Wu, W., El Naggar, M., Mei G., L.R., 2019. Dem analysis of the sand plug behavior during the installation process of open-ended pile. Computers and Geotechnics 109, 23–33. doi:10.1016/j.compgeo.2019.01.014.

Mokrani, L., 1991. Simulation physique du comportement des pieux à grande profondeur en chambre de calibration. Ph.D. thesis. Grenoble INPG.

Rajaï, F., Jean, M., Moreau, J., Roux, S., 1996. Force distribution in dense two-dimensional granular systems. Physical Review Letters 77, 274–277.

Roux, J., Chevoir, F., 2005. Discrete numerical simulation and the mechanical behavior of granular materials. Bulletin des laboratoires des ponts et chaussées 254, 109–138.

Roux, J., Combe, G., 2010. How granular materials deform in quasistatic conditions, in: J. D. Goddard, J. T. Jenkins, P.G. (Ed.), IUTAM-ISIMM Symposium on Mathematical Modeling and Physical Instances of Granular Flow, AIP Conference Proceedings (vol. 1227). p. 260.

Saada, A., Bianchini, G., 1988. Constitutive equations for granular non-cohesive soils - Proceedings of the international workshop on constitutive equations for granular non-cohesive soils. Balkema, Rotterdam, 22-24 July 1987, Cleveland.

Sibille, L., Benahmed, N., Darve, F., 2021. Constitutive response predictions of both dense and loose soils with a discrete element model. Computers and Geotechnics 135, 104161. doi:https://doi.org/10.1016/j.compgeo.2021.104161.

Sibille, L., Villard, P., Darve, F., Aboul Hosn, R., 2019. Quantitative prediction of discrete element models on complex loading paths. International Journal for Numerical and Analytical Methods in Geomechanics 43, 858–887.

Šmilauer, V., Catalano, E., Chareyre, B., Dorofeenko, S., Duriez, J., Dyck, N., Elias, J., Er, B., Eulitz, A., Gladky, A., et al., 2015. Yade documentation 2nd ed. the yade project.

Villard, P., Huckert, A., Briançon, L., 2016. Load transfer mechanisms in geotextile-reinforced embankments overlying voids: Numerical approach and design. Geotextiles and Geomembranes 44, 381–395. doi:10.1016/j.geotexmem.2016.01.007.

Wesley, L.D., 2002. Interpretation of calibration chamber tests involving cone penetrometers in sands. Géotechnique 52, 289–293. doi:10.1680/geot.2002.52.4.289.

Zentar, R., Hicher, P.Y., Moulin, G., 2001. Identification of soil parameters by inverse analysis. Computers and Geotechnics 28, 129–144.

Zhao, S., Evans, T., Zhou, X., 2018. Effects of curvature-related dem contact model on the macro-and micro-mechanical behaviours of granular soils. Géotechnique 68, 1085–1098.

Zitouni, Z., 1988. Comportement tridimensionnel des sables. Ph.D. thesis. Université Joseph Fourier - Grenoble 1. Grenoble, France.